ELSEVIER

Chemical Engineering Science 63 (2008) 1626–1635

Chemical Engineering Science

www.elsevier.com/locate/ces

Mechanisms of formation of iron precipitates from ferrous solutions at high and low pH

Mfandaidza Hove*, Robert P. van Hille, Alison E. Lewis

Department of Chemical Engineering, University of Cape Town, Private Bag, Rondebosch 7701, South Africa

Received 31 August 2007; received in revised form 6 November 2007; accepted 11 November 2007
Available online 19 November 2007

Abstract

The oxidation and subsequent precipitation of iron from solutions are very important for most hydrometallurgical wastewater treatment practitioners. The particle formation process mechanisms are important for shaping the dewaterability and particle size distribution of the precipitates. In this study the objective is to elucidate the mechanisms of iron particles formation from ferrous solutions at high (pH 9.0) and low pH (pH 6.0). The results obtained showed that the precipitation process is dominated by nucleation at the initial stages and aggregation dominated at the final stages. The precipitates formed at higher pH transform faster and result in the formation of more stable precipitates. Precipitates formed at pH 6.0 are larger but less stable chemically. The results may mean higher throughputs and lower costs of post precipitation stabilisation for operations at higher pH. The benefits for operation at lower pH would be a better solid–liquid separation due to the bigger sized particles formed.

Keywords: Iron oxidation; Precipitation mechanism; Wastewater treatment; Phase transformation

1. Introduction

The effective treatment of hydrometallurgical wastewaters, especially acid mine drainage, depends largely on the oxidation and precipitation of iron. This is especially true for South Africa where it has been found that the major metal in acid mine drainage is iron (Pulles et al., 1996). The removal of other metals by co-precipitation and/or adsorption depends on the nature of the iron precipitates initially formed. Most plants employ hydroxide addition to neutralise the wastewaters and at the same time cause the precipitation of iron as a hydroxide. However, before the onset of ferric precipitation, the ferrous iron has to be oxidised to the ferric state, usually by bubbling air through the acid mine drainage solution. The oxidation and subsequent precipitation is done at pH 8.5–9.5 (Cominco Engineering Services, 1997; Brown et al., 2002). Under these high pH conditions, the oxidation of ferrous iron is very rapid and this leads to the formation of complex mixtures of iron species. The concentration of solids from the sedimentation process rarely exceeds 4%. The cause of this poor settling, clarification and reduced potential for thickening and filtration lies in the structure of the precipitates formed. Thus a good understanding (which is currently not the case (Loan et al., 2002; Gan et al., 2005) of the precipitation mechanism of these particles is critical to the optimal precipitation of iron in wastewater treatment. Besides, the precipitates formed are voluminous, gelatinous and therefore need considerable areas of land for disposal. The long-term stability of these precipitates has been questioned, especially with respect to their amphoteric nature.

Most studies carried out on iron precipitation in relation to wastewater treatment have focused on the improvement of the solids density (Kostanbader and Haines, 1970; Bosman, 1974) without investigating the mechanisms responsible for the particle formation processes. This has resulted in the so-called high density sludge (HDS) process. Notwithstanding the improvements gained from the investigations cited above, the HDS process remains one of the most common iron removal processes, yet least mechanistically understood. While some of the studies were concerned with solids densification (as cited above) others (Stumm and Lee, 1961; Sung and Morgan, 1980,

* Corresponding author. Tel.: +27 21 6502511; fax: +27 21 6505501.
E-mail address: mfandaidza.hove@uct.ac.za (M. Hove).

0009-2509/$ - see front matter © 2007 Elsevier Ltd. All rights reserved.
doi:10.1016/j.ces.2007.11.016

Tamura et al., 1976a, b; Dousma and de Bruyn, 1978; Van Der Woulde and De Bruyn, 1983a, b) focused on the oxidation of ferrous iron in natural environments, where the concentrations are very low compared to acid mine drainage. In these studies, the pH was 6 or lower, which is lower than what is usually employed in the treatment of wastewaters. In their studies, Van Der Woude and De Bruyn (1983a, b) found very small particles that were growth limited to 3–5 nm. Pavlides (1995), in another study, found particles in the same size range and concluded that the size of these particles was insensitive to changes in pH in the range 2.5–4.5. The formation of these nanosize particles is very critical in the operation of iron precipitation plants since the removal of other metals by adsorption and/co-precipitation depends on the nature of these iron precipitates. Studies that have been done at high pH and high ferrous iron concentrations resulted in the formation of lepidocrocite via green rusts (Schwertmann and Fechter, 1994), lepidocrocite and schwertmannite (Jönsson et al., 2005, 2006) which is in contrast to the ferrihydrite obtained in the earlier mentioned studies. Other studies (Gan et al., 2005; Loan et al., 2002; Georgaki et al., 2004) investigated the conditions and processes that enhanced the densification of the iron sludge without looking at the processes that were responsible for the formation of the primary particles and sizes of these primary particles. This study is focused on the mechanisms of formation of the primary particles, the stability of these particles and the possible impact of these particles on the effectiveness of precipitation as a process technique for the treatment of hydrometallurgical wastewaters.

2. Techniques and experimental methods

2.1. Technique for studying particle processes

A technique that is often used to make inferences about particle formation processes during precipitation is based on the moment transformation of the number density function $n(L)$ which is obtained by integrating the same with respect to the size of the particles L. Thus the jth moment becomes

$$mj = \int_0^\infty L^j n(L)\,\mathrm{d}L. \tag{1}$$

The symbols L, $n(L)$ and mj represent the size of the particles, the number density function of particles of size L and the moment, respectively. From the integration of the term above the moments obtained are zeroth moment (m_0), first moment (m_1), second moment (m_2) and third moment (m_3), which are proportional to the total number of particles, total length of particles, total surface area of particles and total volume of particles, respectively (Randolph and Larson, 1988; Bramley et al., 1996).

When these moments are computed, they give a single important point for each of the samples taken during the course of the reaction. A plot of the moments against time reveals the active precipitation mechanisms. This technique has been successfully used by Lewis and Ntuli (2006), Andreassen and Hounslow (2004) and Randolph and Larson (1988). Assuming size independent growth and aggregation and absence of breakage, the molecular growth rate (G_0), aggregation kernel (β) and the aggregation rate (R_a) are given by Eqs. (2), (3) and (4) respectively (Randolph and Larson, 1988):

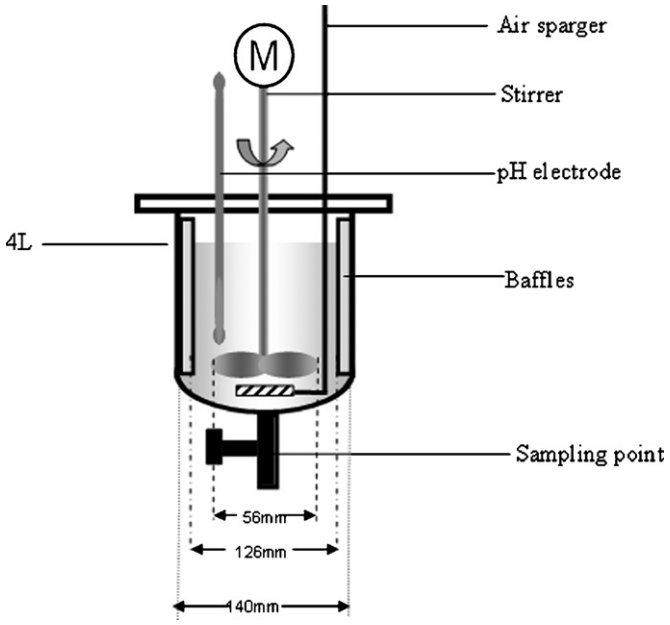

Fig. 1. Experimental setup.

$$G_0 = \frac{\Delta m_3}{3\,\Delta t\,\overline{m_2}}, \tag{2}$$

$$\beta = \frac{\Delta m_2}{\Delta t\,(\overline{m_1})^2} - 2\frac{G_0}{\overline{m_1}}, \tag{3}$$

$$R_a = -\frac{\beta m_0^2}{2}. \tag{4}$$

Eqs. (1)–(4)were used to compute the respective process rates.

2.2. Experimental methods

All the experiments were carried out in a 4 L batch reactor as shown in Fig. 1. The reactor had four equally spaced baffles in order to maximise mixing. The agitator was fitted with a Rushton turbine, and a speed of 350 rpm was used for all the experimental runs. The top of the reactor was covered by a lid with ports for electrodes to measure pH, dissolved oxygen concentration, redox potential and another port for sample collection.

The reactor was first filled with 4 L of deionised water which was then deoxygenated using nitrogen. The pH was adjusted to the preset level by means of a custom made pH stat system using a Hitech Micro Systems controller and Hanna MA911 pH electrode by injecting either 0.05 M H_2SO_4 or 0.1 M NaOH. The pH stat was calibrated against a commercial Hanna 211 m coupled to a Hanna MA911 electrode using commercial pH buffer solutions. The accuracy of the pH stat was 0.1 pH units. Dissolved oxygen concentration was monitored by an YSI 5739 electrode coupled to an Hitech Micro Systems controller. Iron at a concentration of 200 mg/L was then added as $FeSO_4{\cdot}7H_2O$.

The air supply was then opened up to a flow rate in excess of the stoichiometric oxygen requirements.

Samples were collected using a syringe and quickly quenched with 1 M H_2SO_4 and deoxygenated using nitrogen to stop oxidation. One part of the sample was filtered through 0.45 μm filter paper. The filtrate was analysed for dissolved iron (Fe^{2+} and Total Fe) using a Merck Spectroquant® NOVA 60. The procedure for iron analysis was based on the 1-10 phenanthroline method (APHA, AWWA, WEF, 1998). The concentration of Fe^{3+} was found by difference. The other part of the sample was washed several times with deionised water to remove excess ions and then freeze dried for 48 h. The freeze dried solids were dispersed in deionised water, the pH was then corrected to that of the experimental conditions using either NaOH or H_2SO_4 and put in an ultrasonic bath for 5 min. The solids were then analysed for particle size distribution using a Zetasizer Nano ZS series. The phases were identified using X-ray diffraction (XRD), diffuse reflectance infrared fourier transform (DRIFT) spectroscopy techniques and acidified ammonium oxalate (AAO), extraction (Cornell and Schwertmann, 1996). A portion of these solids was digested in order to determine the amount of iron in the solids for purposes of computing a material balance on iron.

3. Results and discussion

3.1. Oxidation of Fe^{2+}

The plot of the Fe^{2+} concentration remaining in solution as a function of time for pH 6.0 and 9.0 is shown in Fig. 2. The plots indicate the rate of oxidation to be higher at pH 9.0 than at pH 6.0 as expected from the rate laws found by Stumm and Lee (1961). The average rate of oxidation at pH 9.0 was found to be 9.8 mg (Fe^{2+})/L/ min. This is significantly lower compared to a rate of 44 100 mg(Fe^{2+})/L/ min that would be predicted from literature based calculations (Stumm and Lee, 1961). This reduced rate could be due to the increased complexity of iron speciation at higher pH (Blesa and Matijevic, 1989). It is also known that SO_4^{2-} (which is a dominating ion in this case) reduces the rate of Fe^{2+} oxidation (Sung and Morgan, 1980; Tamura et al., 1976a). For the pH 6.0 case, the average rate of oxidation was found to be 2.1 mg (Fe^{2+})/L/ min compared to 0.044 mg (Fe^{2+})/L/ min prediction from literature. The reason for the higher than expected rate was due to the catalytic effect of ferrihydrite solids in the pH range 6.0–7.0 as found by Tamura et al. (1976b) and Sung and Morgan (1980). The rapid initial drop in Fe^{2+} concentration (first 10 min at pH 9.0 and first 40 min at pH 6.0) could have been due to direct aqueous oxidation while the less rapid rates towards the end of the reaction could have been due to transformation reactions involving Fe^{2+}/Fe^{3+} metastable complexes and/or Fe^{2+} adsorbed on the ferrihydrite surface.

3.2. Particle size evolution

3.2.1. Solids formed after 5 min of reaction

The particle number distribution, N (#/m^3) of the particles formed after 5 min of reaction is shown in Fig. 3. The inset shows the particle size distribution at pH 6.0. In both cases (pH 6.0 and 9.0) the particle size distribution showed a bimodal distribution. The peaks were at 1280 and 4800 nm at pH 6.0. The distribution at 9.0 showed the formation of smaller particles with peaks at 190 and 712 nm. That the distribution was bimodal was confirmed by a volume based distribution (Fig. 4). It is most likely that two peaks corresponded to crystals of different phases than to crystallites and aggregates of the same phase. This is confirmed by the SEM photographs which show the presence of at least two different phases (Fig. 5). The picture marked A corresponds to the precipitate formed at pH 6.0, while B corresponds to that formed at pH 9.0. In both cases the two different phases are clearly distinguishable. The wide span of the distribution in both cases agreed with the initial formation of monomer species which condense into larger polymeric species by an aggregative mechanism (Flynn, 1984;

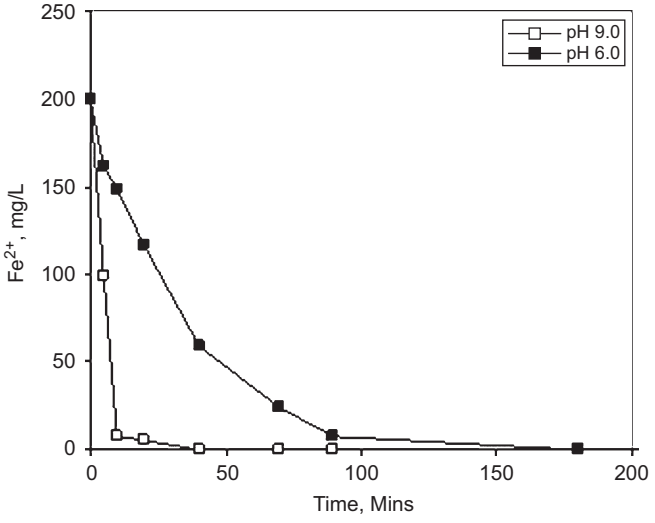

Fig. 2. Fe^{2+} remaining in solution as a function of time at pH 6.0 and 9.0.

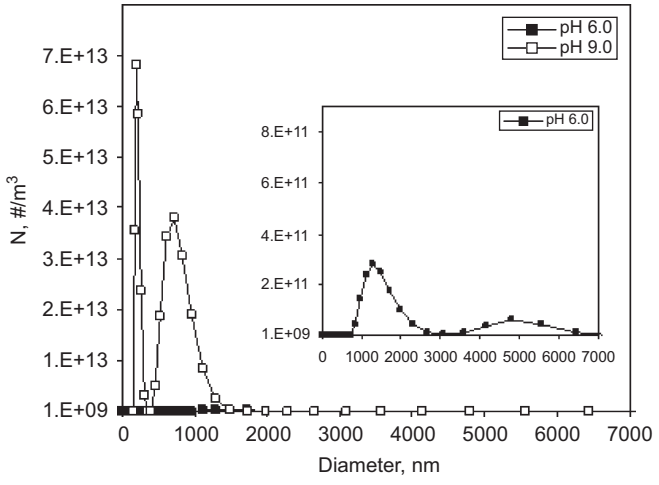

Fig. 3. Particle size distribution after 5 min of reaction. The inset shows the distribution for the pH 6.0 case.

Dousma and de Bruyn, 1978). The open structure of the particles indicated that the solids were made up of mainly amorphous ferrihydrite while traces of green rusts were picked up by XRD analysis at pH 9.0. The presence of lepidocrocite as indicated by the DRIFT analysis also indirectly confirms the formation of green rusts since it is known that lepidocrocite is formed via green rusts (Cornell and Schwertmann, 1996; Schwertmann and Fechter, 1994; Jolivet et al., 2004). The decreased size of the particles at pH 9.0 was due to the increased oxidation rate which resulted in high primary nucleation rates and depressed growth of the particles. These conditions of high oxidation rate (Fig. 2) support high supersaturation levels, resulting in the formation of thermodynamically less stable but kinetically favoured ferrihydrite and green rusts (Jambor and Dutrizac, 1998; Loan et al., 2006). It is because of the high oxidation rates that the number of particles formed also increased significantly at pH 9.0 compared to pH 6.0 (Fig. 3). In both cases the size of the particles obtained was larger than the limiting colloid size reported by Van Der Woude and De Bruyn (1983b) of 3–5 nm. This could have been due to the high pH (more base) which induced deprotonation of the polynuclear species and led to coagulative aggregation. However, at pH 9.0 it would seem that the rate of deprotonation was lower than the rate of nucleation; hence smaller particles were formed although there was more base compared to pH 6.0. The other reason for the bigger particles at pH 6.0 is that this is closer to the point of zero charge of most iron oxide hydroxide which is around pH 7.0 (Schwertmann and Cornell, 2000). This could have caused Van der Waals forces induced flocculation. The bimodal distribution obtained is typical of mixed phase systems, supporting the view that different iron phases were formed during the initial stages of the reaction.

3.2.2. Solids formed after 20 min

The particle size distribution for solids formed after 20 min of reaction is shown in Fig. 6. The precipitate that had formed after 20 min at pH 6.0 showed high polydispersity with modal peaks at 396, 1720 and 4800 nm. The number distribution of the particles formed at pH 9.0 had a modal peak of 396 nm. Smaller particles were in higher proportion than after 5 min of reaction at both pH 6.0 and 9.0 which was a result of continued nucleation but with less chain elongation because of

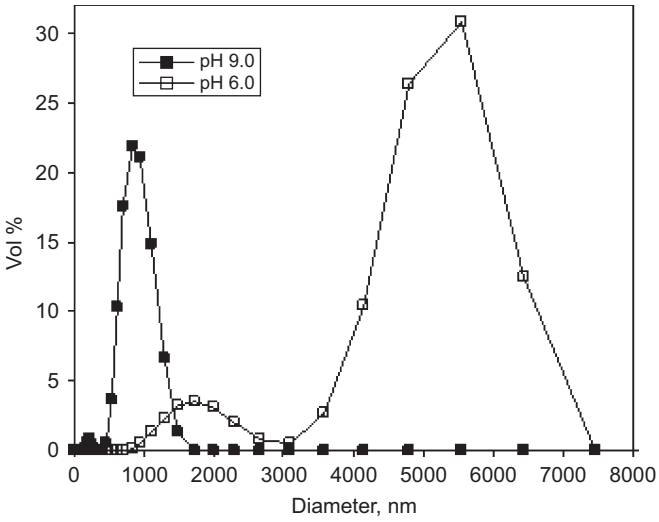

Fig. 4. Volume based particle size distribution after 5 min of reaction.

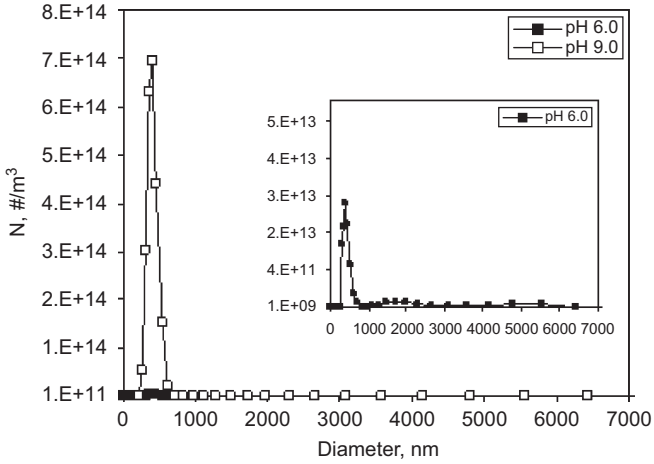

Fig. 6. Particle size distribution after 20 min of reaction. The inset shows the distribution for the pH 6.0 case.

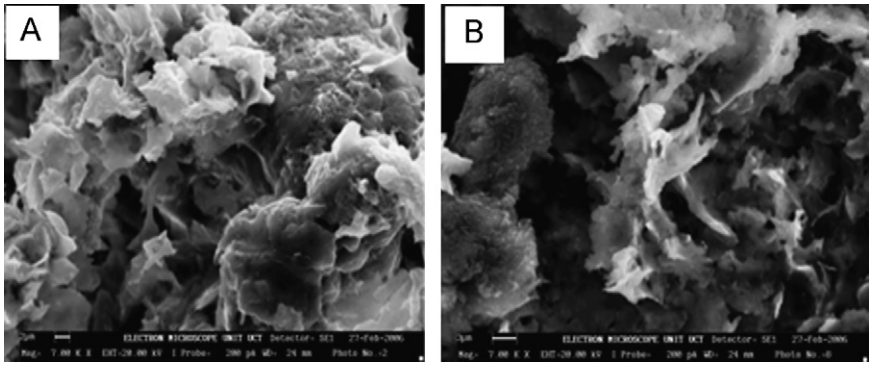

Fig. 5. SEM pictures of the precipitates formed after 5 min of reaction. (A) Precipitate formed at pH 6.0 and (B) precipitate formed at pH 9.0.

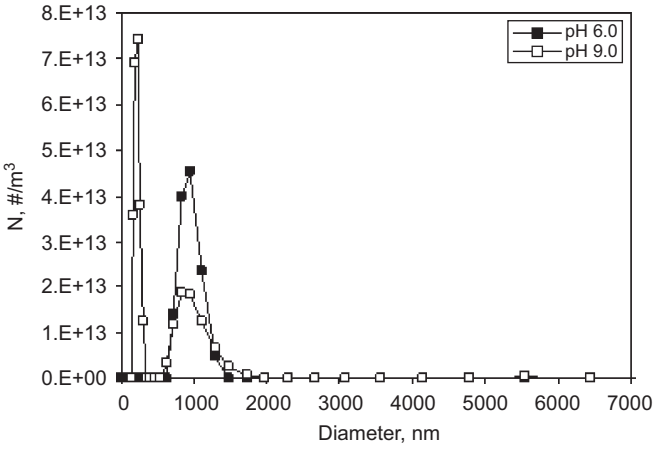

Fig. 7. Particle size distribution after 40 min of reaction.

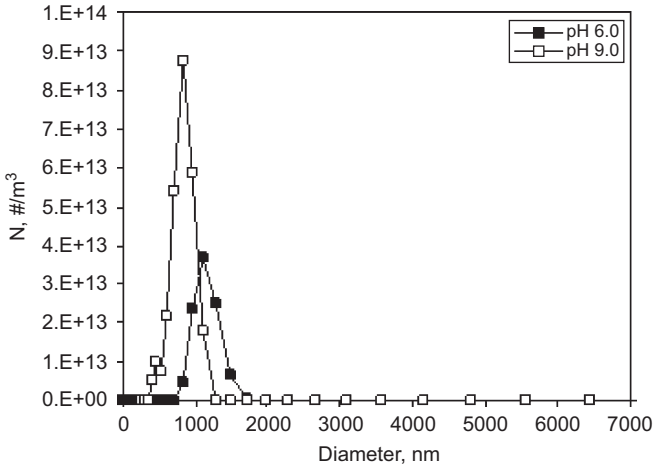

Fig. 8. Particle size distribution after 90 min of reaction.

decreased supersaturation due to decreased oxidation rates. The change in the distribution compared to solids formed after 5 min could also be due to the formation of green rusts and transformation of polymeric ferrihydrite phases. It is also known that the big ferrihydrite flocs can be disrupted by ageing and stirring through the expulsion of free water molecules (Gan et al., 2005). Although the XRD spectra were very complex, an automatic search and match showed the possible presence of green rusts for the pH 9.0 case (Fig. 19). Again, as after 5 min of reaction the particles formed at pH 9.0 were relatively smaller and higher in number compared to particles formed at pH 6.0.

3.2.3. Solids formed after 40 min of reaction

The particle size distribution is shown in Fig. 7. The particle size distribution of the solids formed at this stage of the reaction showed a narrower monomodal distribution at pH 9.0 (Fig. 7). The modal peak at pH 6.0 was 955 nm, while two peaks (122 and 459 nm) were obtained at pH 9.0. The disappearance of the larger particles previously obtained at pH 6.0 was as a result of solution mediated transformation of the green rusts as air continued to be bubbled through the reactor. The disappearance of the same large size particles at pH 9.0 took place after 20 min of reaction. XRD analysis confirmed the absence of green rusts in both the pH 9.0 and the pH 6.0 precipitates at this stage of the reaction. This disappearance of the bigger particles cannot be attributed to dissolution because the concentration of dissolved iron continued to decrease during the course of the reaction. The zeroth moment also increased (see Fig. 11), which supports the view that there was nucleation of 'new' iron species. From this it can be concluded that the transformation of less stable species into more crystalline phases takes place in both cases but with the onset of the same coming earlier at pH 9.0 than at pH 6.0. From a wastewater treatment operation point of view this could mean that it is more beneficial (disregarding the increased mean particle size) to oxidise iron at pH 9.0 as this results in a more stable precipitate compared to oxidation at pH 6.0.

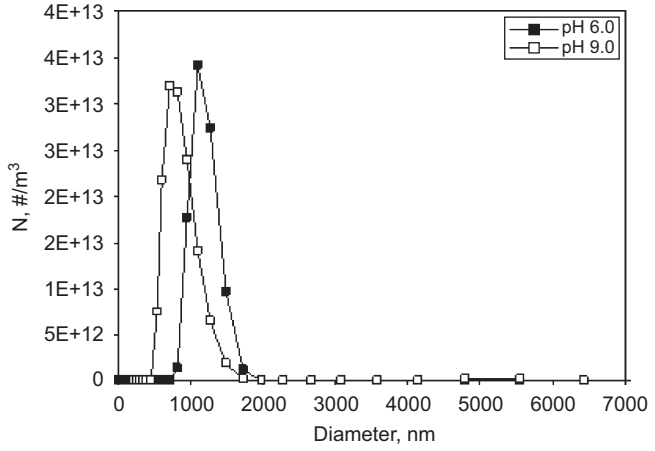

Fig. 9. Particle size distribution after 180 min of reaction.

3.2.4. Solids formed after 90 min of reaction

The particle size distribution for the precipitate formed after 90 min of reaction is shown in Fig. 8. The number distribution of the particles was monomodal with peak height at 1110 and 712 nm for pH 6.0 and 9.0, respectively. The disappearance of the smaller size particles compared to the previous distributions and the increase in the modal size showed that the active size enlargement mechanism was aggregation.

3.2.5. Solids formed after 180 min of reaction

The number distribution of the particle size was monomodal with peak at 1110 and 712 nm, just as in the previous case (Fig. 9). The number of particles was slightly higher for pH 6.0 than for pH 9.0. The fact that the modal size after 180 min was the same as the modal size after 90 min indicated that a state of dynamic equilibrium between particle breakage and aggregation could have been reached.

3.2.6. Solids formed after 1440 min (24 h) of reaction

The size distribution was narrower and monomodal (Fig. 10) with modal height at 1720 and 1280 nm for pH 6.0 and 9.0,

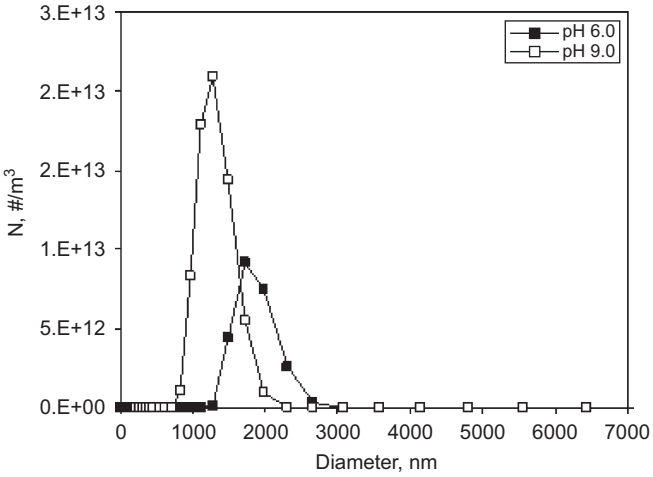

Fig. 10. Particle size distribution after 1440 min of reaction.

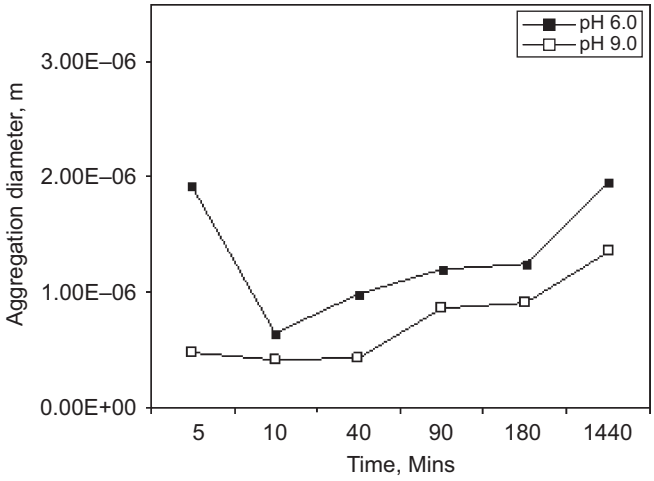

Fig. 12. Evolution of the population based mean size $\overline{L_{1,0}}$ during the course of the reaction.

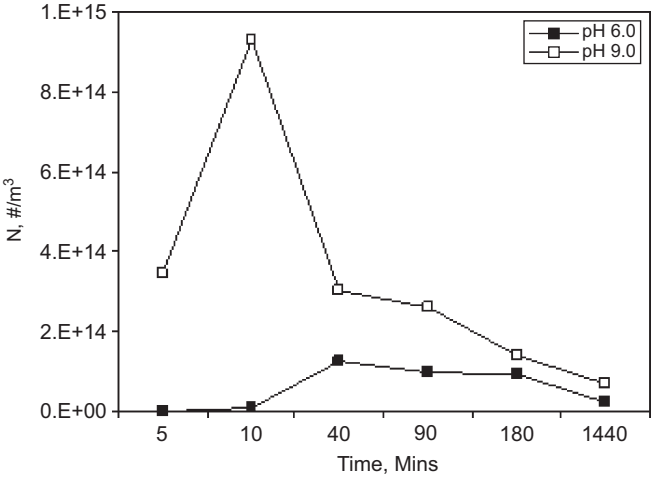

Fig. 11. Evolution of m_0 during the course of the reaction.

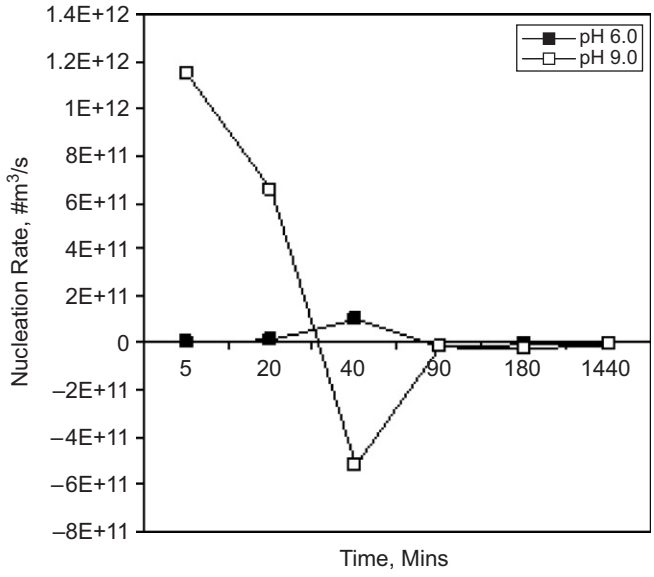

Fig. 13. Change in the nucleation rate with time for the two pH cases.

respectively. In both cases there was a marked increase in the modal size of the particles accompanied by a corresponding decrease in the number of particles, a sure confirmation of the flocculation of the particles caused by Van der Waals forces. While supersaturation induced aggregation cannot be ruled out, the non-availability of dissolved iron supports electrostatic forces for the size enlargement.

3.2.7. Evolution of number of particles (m_0) and mean size of particles ($\overline{L_{1,0}}$)

The evolution of the zeroth moment (m_0) is shown in Fig. 11. The increase in the total number of particles up to 40 min in both cases was due to nucleation. While breakage would have a similar effect on m_0, this is unlikely to be the cause of the cited observation since there was always a corresponding decrease in the amount of iron in solution which indicated consumption of supersaturation. The decrease in m_0 at pH 9.0 from 40 to 90 min was sharper than at pH 6.0. This indicated that the aggregation rates were higher at pH 9.0 than at pH 6.0 since aggregation or dissolution are the only mechanisms responsible for a decrease in the number of particles. From 90 to 180 min there was a slight change in m_0 in both cases showing that the particles had reached their limiting aggregative size under the prevailing hydrodynamic conditions. The further reduction in m_0 after 1440 min was due to the absence of shear induced particle breakage since agitation was stopped after 180 min of reaction.

The change in the population based mean size $\overline{L_{1,0}}$ of the particles as a function of time is shown in Fig. 12. In both cases the initial decrease in $\overline{L_{1,0}}$ from 5 to 20 min was due to high rates of nucleation (Fig. 13) at the expense of growth and aggregation (Claassen and Sanderbergh, 2006). The sharper drop in the average size for the pH 6.0 case was due to the increase in the nucleation rate as shown on Fig. 13. From 20 min up to 90 min the mean particle size increased due to aggregation.

This is supported by a corresponding decrease in m_0 for both cases. The near constant mean particle size between 90 and 180 min again showed that the system could have reached a state of dynamic equilibrium between particle breakage or attrition and aggregation. The further increase in size after 1440 min indicated that shear stresses under stirred conditions were responsible for limiting the size of particles through shear induced breakage. In conclusion, therefore, the formation of ferrihydrite particles at high pH is dominated by nucleation at the initial stages followed by limited growth. Aggregation dominates after the oxidation stage has been completed.

Although the average particle sizes were different for the two cases, there was no significant difference in solids density of the precipitates. The solids densities (m/v) were 0.87% and 0.85% for the pH 6.0 and 9.0, respectively. From these values, the implication is that it is more favourable to operate these processes at the higher pH and thereby benefit from the kinetic advantages, given that the settling behaviour hardly changes with pH.

3.3. Evolution of precipitation kinetic processes

3.3.1. Evolution of the nucleation rate

The change in the average nucleation rate is shown in Fig. 13. The results were obtained by dividing the m_0 by time. Only positive nucleation rates were considered in the discussions that follow. Negative values were taken to mean that nucleation was not a dominant kinetic process for that particular instance, although it has to be noted that the same could be significant. In all instances the nucleation rate was higher for the pH 9.0 case than for the pH 6.0 case. This is in agreement with particle size distribution results shown in the earlier sections. This also shows that at higher pH, higher oxidation rates prevail resulting in higher supersaturation levels. After 20 min, nucleation rate calculations at pH 9.0 gave negative values, implying that the rate of crystal birth by nucleation was lower than death by agglomeration. For the pH 6.0 case this happened after 40 min, again showing that the nucleation kinetics are slower at lower pH than at higher pH. The order of magnitude of these results can be compared with those obtained by Van Der Woude and De Bruyn (1983b). The comparison shows that the rates of nucleation obtained here are relatively high. It can also be deduced that the reaction is nucleation dominated at the initial stages, with the same decreasing slightly with time in correspondence with the depletion of iron from solution. The slight increase in the nucleation rate (for the pH 6.0 case) after 40 min was probably due to transformation processes.

3.3.2. Evolution of the growth rate

The growth rates calculated for both cases covered the entire experimentation time. The results for the change in the growth rate are shown in Fig. 14. Up to 90 min the growth rate at pH 6.0 was higher than at pH 9.0. This is expected since low supersaturation, which was experienced at low pH promotes growth at the expense of nucleation. The very low growth rates of the order of 1×10^{-17}–1×10^{-10} m/s obtained show that the precipitation of iron from ferrous sulphate solutions is growth limited, more so at higher pH. The decrease in the growth rates with time was probably to the exhaustion of supersaturation from the solution.

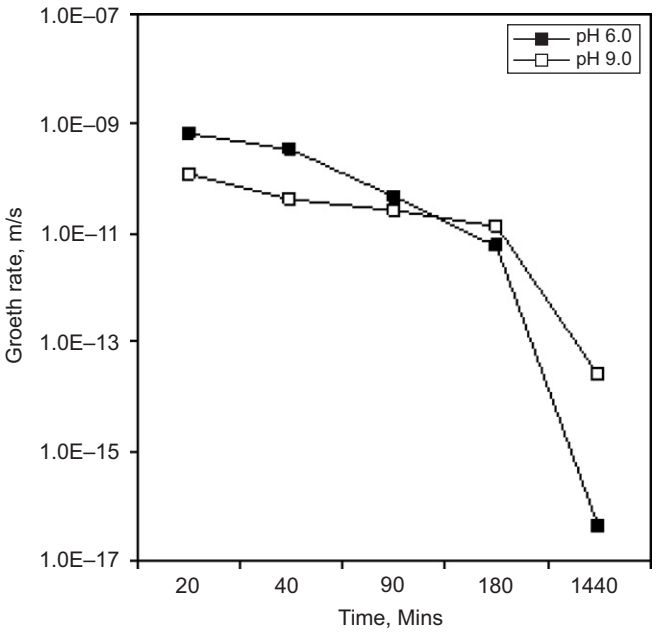

Fig. 14. Change in the molecular growth rate (G_0) with time during the course of the reaction.

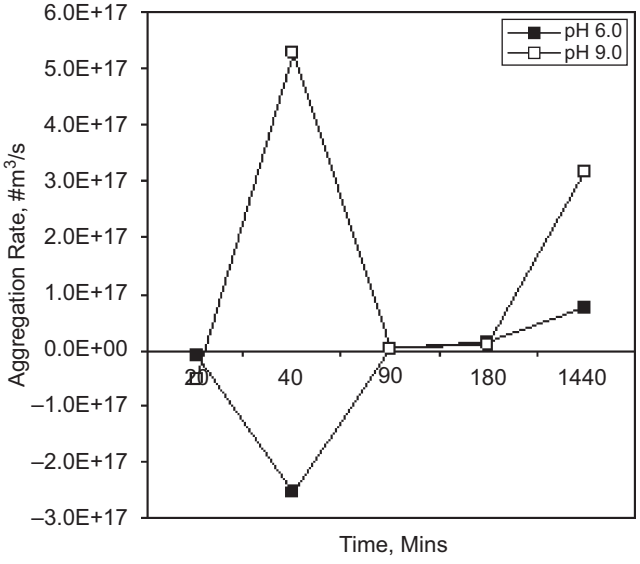

Fig. 15. Change in the aggregation rate (R_a) with time during the course of the reaction.

3.3.3. Evolution of the aggregation rate

The change in the aggregation rates with time for both experimental cases is shown in Fig. 15. The aggregation rates for the pH 9.0 case were higher than for the pH 6.0 case. This is because the m_0 values at pH 9.0 were higher than those at pH 6.0 (aggregation rate is a function of the square of m_0). From the beginning of the experiment up to 40 min (for the pH 6.0

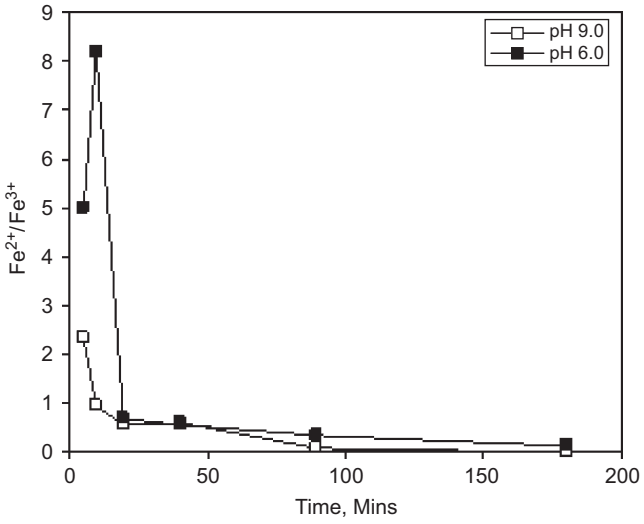

Fig. 16. Evolution of the Fe^{2+}:Fe^{3+} ratio during the course of the reaction.

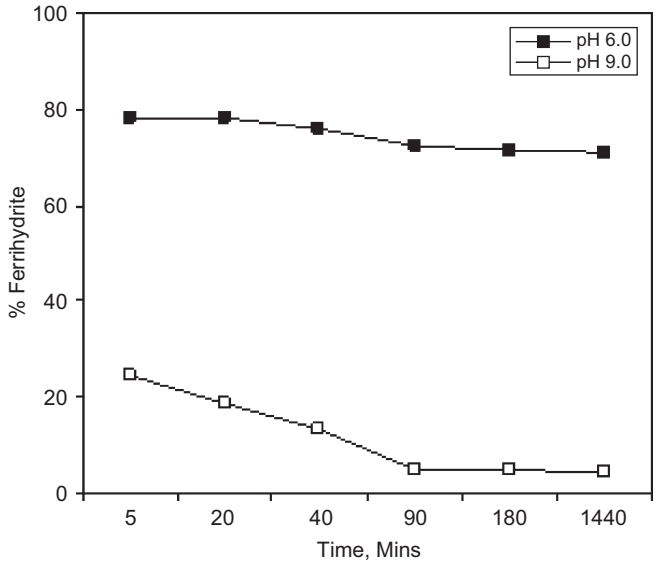

Fig. 17. Evolution of ferrihydrite composition with time.

case), negative aggregation rate values were obtained. Like in the nucleation rate case, it has to be noted that the negative values meant aggregation was not the dominant particle formation mechanism but it could be significant. This showed that during these early stages of the reaction aggregation was not a dominant particle formation mechanism. There after, the aggregation rate increased from 2.5×10^{15} # m^{-3} s^{-1} after 90 min to 7.6×10^{16} # m^{-3} s^{-1} after 1440 min. This is an unexpected result under classical precipitation kinetics because when m_0 decreases and $\overline{L_{1,0}}$ decreases, then the aggregation rate should also decrease. The decrease in m_0 and increase in $\overline{L_{1,0}}$ without an accompanying decrease in the aggregation rate can probably be explained in terms of solution transformation. In the earlier sections it was shown that there was a disappearance of the bigger particles although the population based size continued to increase. This dissolution reprecipitation of the iron species could probably be responsible for the anomalous trend in the aggregation rate.

These dissolution and reprecipitation processes can also be explained in terms of the evolution of Fe^{2+} and Fe^{3+} composition in the precipitate during the course of the reaction. This is shown in Fig. 16. During the first 10 min of the reaction, the proportion of Fe^{2+} was higher than that of Fe^{3+} (the ratio Fe^{2+}/Fe^{3+} being higher than 1). It should be noted that the presence of Fe^{2+} in the solid particles represents some level of thermodynamic instability. For the pH 9.0 case, the Fe^{2+}/Fe^{3+} ratio was higher than 1 in the first 10 min, gradually decreasing to less than 1 after 20 min and finally reaching 0 at 90 min. For the pH 6.0 case, the Fe^{2+}/Fe^{3+} ratio sharply increased at 10 min and thereafter decreased to 0.1 at 90 min. XRD analyses done on the samples showed the presence of unstable green rusts during the early stages of the reaction in both cases. These green rusts disappeared at the later stages of the reaction. Ferrihydrite was found to be the major component in the final precipitate for the pH 6.0 case while goethite and lepidocrocite were the major phases for the pH 9.0 case (Fig. 17). The Fe^{2+}/Fe^{3+} ratio shows that although the particles formed at pH 6.0 are bigger and easier to separate, they are less stable compared to those formed at pH 9.0. Thus although there was no detectable soluble iron in solution, the presence of Fe^{2+} in the precipitate means that this could provide surface supersaturation that could result in further nucleation or growth or aggregation or all of these processes. This could probably be the explanation for the anomalous trend obtained for the aggregation rates. The other implication, especially for wastewater treatment operations, is that it would be better to operate treatment plants at higher pH as this would ensure the formation of more stable precipitates that may not require post precipitation stabilisation.

3.3.4. Transformation of the precipitates

The transformation of the precipitates was inferred from the evolution of the amorphous components in the solid. The technique is based on the fact that ferrihydrite dissolves in AAO while the crystalline phases do not. To carry out this test, 0.2 M ammonium oxalate was buffered to pH 3.0 by the use of 0.2 M oxalic acid. A known amount of precipitate was digested in this solution for 2 h in the dark. The amount of iron in solution was determined using the spectroquant.

The proportion of ferrihydrite was calculated using the equation below:

$$\%\text{Ferrihydrite} = \frac{Fe_{AAO}}{Fe_{Tot}} \times 100, \tag{5}$$

where Fe_{AAO} represents the amount of iron soluble in AAO and Fe_{Tot} represents total iron found by digestion in concentrated HCl.

The results for the two pH cases are shown in Fig. 15. The figure shows that at pH 6.0 the major component (70%) of the precipitate was amorphous ferrihydrite. The DRIFT results showed that the crystalline part of this precipitate was lepidocrocite (Fig. 18). The transformation of the precipitate at pH 6.0 thus consisted of the conversion of green rusts into

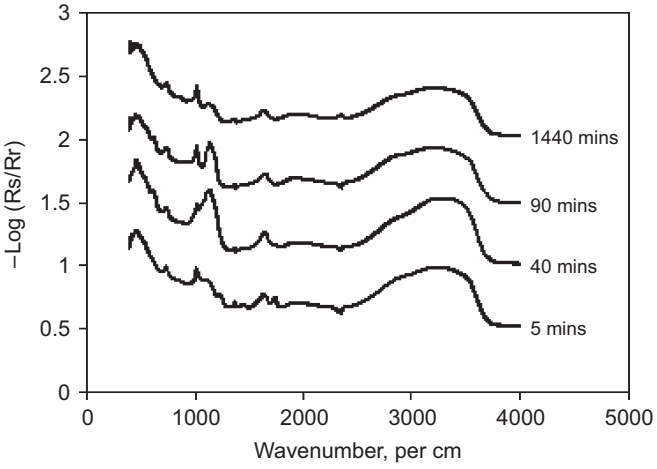

Fig. 18. DRIFT spectra of the precipitate formed under pH 6.0 conditions.

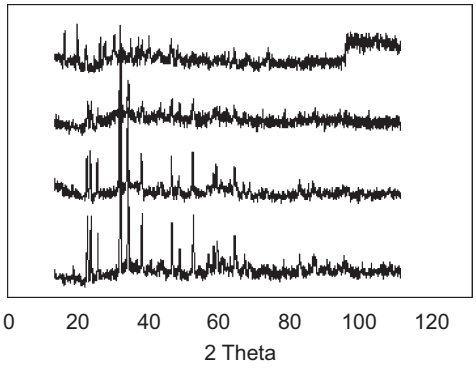

Fig. 19. XRD spectra of the precipitate formed under pH 9.0 conditions.

lepidocrocite (constituting about 30% of the final product) and ageing of the ferrihydrite itself into a more ordered form. These two transformation processes were probably responsible for the disappearance of the bigger particles for the pH 6.0 case from the particle size distributions shown earlier (Figs. 3, 6 and 7). Considering the pH 9.0 case, amorphous ferrihydrite constituted about 25% after 5 min and about 5% at the end of the reaction after 24 h. This means that the evolution of the particle size distribution was due to the transformation of ferrihydrite into goethite and transformation of green rusts into lepidocrocite. The XRD spectra showed that the crystallinity of the precipitate improved with time. Although the spectra was too complex to resolve, an automatic search and match showed the presence of green rusts at the beginning and lepidocrocite and goethite after 24 h. The XRD spectra are shown in Fig. 19. Cornell and Giovanoli (1985) also found that ferrihydrite transformed into goethite at high pH within 24 h. It can therefore be inferred that the major component under these high pH conditions was goethite and not lepidocrocite. This relatively fast transformation of ferrihydrite into goethite could be significant for wastewater treatment engineers. First it means that it will not be necessary to have a post precipitatio stabilisation facility. Secondly operation at higher pH ensures faster kinetics and therefore higher plant throughputs.

4. Conclusion

From results presented here, it is evident that the pH has a profound effect on the particle size distribution of the final precipitation product and the overall process kinetics and hence plant throughput, and the stability of the precipitates formed. High pH promotes high oxidation rates with resultant increased plant throughput and more stable precipitates but with significantly smaller particle size distributions.

The challenge then for the waste water treatment design engineer is two-fold; first whether to effect solid–liquid separation before oxidation is complete and get better solid–liquid separation at the expense of solids stability or allow for complete oxidation and get poorer removals but stable solids. The second scenario is to choose between fast or slow oxidation kinetics. High oxidation rates give a more stable precipitate in a shorter time period and hence higher treatment throughput. On the other hand, slow oxidation kinetics give bigger particles and better removals but less throughput and less stable precipitates. Obviously designers of such plants have the big challenge of striking a balance among all these significantly intertwined parameters. In summary the oxidation precipitation of iron from ferrous solutions can be summarised as consisting of the following process steps:

(1) Rapid initial oxidation of Fe^{2+} and the instantaneous formation of primary particles (nucleation) from Fe^{3+} referred to as polynuclear cationic species (Blesa and Matijevic, 1989). These particles increase in size by a condensation mechanism resulting in the ejection of hydrogen ions (Jolivet et al., 2004). The rate of nucleation increases as the pH increases.
(2) The particles formed above associate with Fe^{2+} from solution through an adsorptive mechanism resulting in the formation of unstable green rusts (Schwertmann and Fechter, 1994) and ferrihydrite flocs with Fe^{2+} possibly adsorbed on them. These are the particles that were responsible for the higher modal sizes observed in the particle size distribution during the early stages of the reaction. Because of faster kinetics, precipitates formed at higher pH take shorter time periods to transform and completely oxidise the Fe^{2+}. This stage of the process is associated with limited growth of the particles and solution mediated transformation of the particles.
(3) The last stage of the process is the aggregation of the particles. In this stage the mainly ferrihydrite particles consume the final traces of supersaturation by an aggregative mechanism at pH 6.0 and through transformation into more crystalline phases at pH 9.0. The final aggregates formed at higher pH have a smaller size due to the initial high nucleation rates compared to the particles formed at lower pH.

Table 1 summarises the active kinetic processes and the effect of pH on these processes as well as on the final product.

From the above scenarios, it can be concluded that the oxidation precipitation of iron involves complex reactions and transformations. This in turn results in complex precipitation

Table 1
Summary of the interactions and active processes in the oxidation precipitation of iron from ferrous sulphate solutions

Kinetic process	pH 6.0	pH 9.0
Nucleation rate	Lower	Higher
Growth rate	Higher (but limited)	Lower (still limited)
Aggregation rate	High	High
Transformation	Slower	Faster
Stability	Lower	Higher
Particle size	Bigger	Smaller

process kinetics where it is difficult to isolate the competing nucleation, growth and aggregation processes. The transformation reactions further complicate these processes. In spite of these difficulties, it has been demonstrated here that by using simple moment transforms techniques and both qualitative and quantitative analytical techniques, inferences could be made on the mechanisms involved in the formation of iron precipitates from high concentration ferrous sulphate solutions at high pH. These results have profound impacts for the wastewater treatment operator in that optimum operational conditions will need a balance among the desired metal removals, throughput requirements, stability issues and dewaterability.

Acknowledgements

The authors thank the financial support from the National Research Foundation and the Water Research Commission.

References

Andreassen, J., Hounslow, M.J., 2004. Growth and aggregation of vaterite in seeded-batch experiments. AICHE Journal 50, 2772–2782.

APHA., AWWA., WEF., 1998. Standard Methods for the Examination of Water and Wastewater. APHA, AWWA, WEF, Washington.

Blesa, M.A., Matijevic, E., 1989. Phase transformations of iron oxides, oxohydroxides, and hydrous oxides in aqueous media. Advances in Colloid and Interface Science 29, 173–221.

Bosman, D.J., 1974. The improved densification of sludge from neutralised acid mine drainage. Journal of the South African Institute of Mining and Metallurgy 340–348.

Bramley, A.S., Hounslow, M.J., Ryall, R.L., 1996. Aggregation during precipitation from solution: a method for extracting rates from experimental data. Journal of Colloid and Interface Science 183, 155–165.

Brown, M., Barley, B., Wood, H., 2002. Minewater Treatment Technology, Application and Policy. IWA Publishing, UK.

Claassen, J.O., Sanderbergh, R.F., 2006. Particle growth parameters in the precipitation of metastable iron phases form zinc-rich solutions. Hydrometallurgy 84, 165–174.

Cominco Engineering Services Limited, 1997. Pilot scale testing of the high density sludge process. Britannia Mine Acid Mine Drainage Treatment Report. Vancouver, BC.

Cornell, R.M., Giovanoli, R., 1985. Effect of solution conditions on the proportion and morphology of goethite formed from ferrihydrite. Clays and Clay Minerals 33, 424–432.

Cornell, R.M., Schwertmann, U., 1996. The Iron Oxides; Structure, Properties, Reactions and Uses. VCH, Weinheim.

Dousma, J., de Bruyn, P.L., 1978. Hydrolysis–precipitation studies of iron solutions II. Aging studies and the model for precipitation from Fe (III) nitrate solutions. Journal of Colloid and Interface Science 64, 154–170.

Flynn, C.M.J., 1984. Hydrolysis of inorganic iron(III) salts. Chemical Reviews 84, 31–41.

Gan, W.Y., Selomulya, C., Tapsell, G., Amal, R., 2005. Densification of iron (III) sludge in neutralisation. International Journal of Mineral Processing 76, 149–162.

Georgaki, I., Dudeney, A.W.L., Monhemius, A.J., 2004. Characterisation of iron-rich sludge: correlations between reactivity, density and structure. Minerals Engineering 17, 305–316.

Jambor, L., Dutrizac, J.E., 1998. Occurrence and constitution of natural and synthetic ferrihydrite, a widespread iron oxyhydroxide. Chemical Reviews 98, 2549–2585.

Jolivet, J.P., Chaneac, C., Tronc, E., 2004. Iron oxide chemistry. From molecular clusters to extended solid networks. Chemical Communications 481–487.

Jönsson, J., Persson, Per., Sjoberg, S., Lövgren, L., 2005. Schwertmannite precipitated from acid mine drainage: phase transformation, sulphate release and surface properties. Applied Geochemistry 20, 179–191.

Jönsson, J., Jönsson, J., Lövgren, L., 2006. Precipitation of secondary Fe (III) minerals from acid mine drainage. Applied Geochemistry 21, 437–445.

Kostanbader, P.D., Haines, G.F., 1970. High density sludge treats acid mine drainage. Coal Age 90–97.

Lewis, A., Ntuli, F., 2006. The effect of a morphology modifier on the precipitation of nickel powder. Chemical Engineering Science 61, 5827–5833.

Loan, M., Newman, O.M.G., Cooper, R.M.G., Farrow, J.B., Parkinson, G.M., 2006. Defining the paragoethite process for iron removal in zinc hydrometallurgy. Hydrometallurgy 81, 104–129.

Loan, M., Parkinson, G., Newman, M., Farrow, J., 2002. Iron oxy-hydroxide crystallization in a hydrometallurgical residue. Journal of Crystal Growth 235, 482–488.

Pavlides, A.G., 1995. The precipitation of iron oxy-hydroxides from ferrous sulphate solution. M.Sc. Thesis, University of Witwatersrand, Johannesburg.

Pulles, W., Heath, R., Howard, M., 1996. A manual to assess and manage the impact of gold mining operations on the surface water environment. WRC Report No. TT79/96, Pretoria.

Randolph, A.D., Larson, M.A., 1988. Theory of Particulate Processes. Academic Press Inc., USA.

Schwertmann, U., Cornell, R.M., 2000. Iron Oxides in the Laboratory, Preparation and Characterization. Wiley-VCH, Weinheim.

Schwertmann, U., Fechter, H., 1994. The formation of green rust and its transformation to lepidocrocite. Clay Minerals 29, 87–92.

Stumm, W., Lee, G.F., 1961. Oxygenation of ferrous iron. Industrial and Engineering Chemistry Research 53, 143–146.

Sung, W., Morgan, J.J., 1980. Kinetics and product of ferrous iron oxidation in aqueous systems. Environmental Science and Technology 14, 561–568.

Tamura, H., Goto, K., Nagayama, M., 1976a. Effect of anions on the oxygenation of ferrous ion in neutral solutions. Journal of Inorganic and Nuclear Chemistry 38, 113–117.

Tamura, H., Goto, K., Nagayama, M., 1976b. The effect of ferric hydroxide on the oxygenation of ferrous ions in neutral solutions. Corrosion Science 16, 197–207.

Van Der Woude, J.H.A., De Bruyn, P.L., 1983a. Formation of colloidal dispersions from supersaturated iron (III) nitrate solutions. I. Precipitation of amorphous iron hydroxide. Colloids and Surfaces 18, 55–78.

Van Der Woude, J.H.A., De Bruyn, P.L., 1983b. Formation of colloidal dispersions from supersaturated iron (III) nitrate solutions II. Kinetics of growth at elevated temperatures. Colloids and Surfaces 8, 79–92.